Transaction A: Civil Engineering
Vol. 16, No. 4, pp. 340–350
© Sharif University of Technology, August 2009

Research Note

SCIENTIA
IRANICA

A Comparison of Three Adaptive Finite Element Refinement Techniques for Incompressible Navier-Stokes Equations Using a CBS Scheme

A. Rahmani Firoozjaee[1],[*] and M.H. Afshar[1]

Abstract. *The numerical solution of incompressible Navier-Stokes equations for flows involving complex geometries is greatly affected by mesh resolution. In these flows, some regions may need finer mesh than others. Adaptive Mesh Refinement (AMR) techniques enable the mesh to be locally refined, based on error distribution in the previous analysis. In this paper, three adaptive refinement methods, namely, Superconvergent Patch Recovery (SPR) based refinement, gradient based refinement and curvature (2nd derivative) based refinement are used in conjunction with the characteristic based split finite element method to solve a benchmark problem of a lid-driven cavity. The results of the proposed adaptive refinement methods are presented and their efficiencies are compared. The results show the effectiveness of the adaptive refinement method for the efficient and accurate simulation of flow problems.*

Keywords: *Adaptive refinement; Characteristic based split; Navier-Stokes; CBS; FEM.*

INTRODUCTION

The Finite Element Method (FEM) is a mesh based numerical method requiring discretization of the computational domain into elements. The size and order of elements used to discretize the problem domain greatly affect the accuracy of the final results. The convergence property of the FEM indicates that the solution to the underlying problem can be improved by either reducing the element size or increasing its order, represented by the order of the shape function used to interpolate the unknowns, leading to two main classes of solution refinement, referred to as h- and p-refinement. Of these, h-refinement is the method widely used by FE practitioners. A uniform refinement of the FE meshes, however, may lead to inefficiency of the method, due to a huge increase in the scale of the problem. A remedy to this problem can be through adaptive refinement, in which the problem domain is only refined in areas with a higher solution error. In simple engineering problems, it is possible to recognize the areas with poor solutions prior to the main analysis by engineering judgment, whereas, in complex problems, it is too difficult and sometimes impossible to predict the areas of higher error before a preliminary solution is found. Error estimate based adaptive refinement methods are efficient tools to generate suitable meshes for the problem using a posteriori error estimate of the finite element results. In these methods, the problem is first solved on an initial mesh designed by engineering judgment. A post-processing of the FE results is then carried out to find the distribution of error on the solution domain, which is subsequently used to create a mesh with elements of smaller size at areas of higher error and vice-versa. The error estimation is an important component of any successful adaptive refinement procedure.

Zienkiewicz and Zhu introduced a very effective recovery process, named superconvergent patch recovery for self adjoint problems such as problems of heat conduction and elasticity [1-4]. This method and its relevant methods have been used in structural design frequently [5-6]. Peralla used a patch recovery method on the velocity-pressure formulation of the steady and incompressible Stokes problem [7]. Recently, Almeida and coworkers used an anisotropic error estimator to solve the Navier-Stokes equations [8]. Cao applied a posteriori error estimator to solve the compressible Navier-Stokes equations [9].

[1] *Department of Civil Engineering, Iran University of Science and Technology, Tehran, P.O. Box 16765-163, Iran.*

[*] *Corresponding author. E-mail: arahmani@IUST.ac.ir*

Received 7 May 2007; received in revised form 21 January 2009; accepted 21 April 2009

On the other hand, it is known that numerical solutions of the incompressible Navier-Stokes equations may suffer from numerical instability if the standard Galerkin procedure is used to discretize the governing equations. This is mostly due to the convective characteristics of the problem, which are normally exhibited in the form of oscillatory solutions. Some methods, such as the Petrov-Galerkin introduced by Zienkiewicz and coworkers [10], the streamline Petrov-Galerkin (SUPG), which is an extension of the Petrov-Galerkin in two and three dimensions [11], the Taylor-Galerkin presented by Donea, which is proved to be the finite element equivalent of the Lax-Wendroff method developed in a finite difference context [12], Galerkin Least Squares (GLS), defined as a linear combination of the standard Galerkin and least squares approximations [13] and Finite Increment Calculus (FIC), presented by Onate [14], are developed to overcome numerical instability due to high convective terms.

Another difficulty arises when solving an incompressible Navier-Stokes equation in its primitive form with the pressure and velocities as the primary unknowns due to the lack of proper equations describing the evolution of the pressure. One of the very popular procedures of dealing with pressure terms in incompressible Navier-Stokes equations is the fractional step or projection method initially presented by Chorin in a finite difference context [15,16].

In this paper, adaptive refinement is used to obtain highly accurate solutions for the Navier-Stokes equations using the Characteristic Based Split-Finite Element Method (CBS-FEM). The Characteristic Based Split Finite Element Method (CBS-FEM) proposed by Zienkiewicz and his coworkers to solve the Navier-Stokes equations is a combination of a fractional step method and a higher order time stepping method developed to overcome the convective term instability. In this work, three error indicators/estimators, named super-convergent patch recovery based error estimator, gradient based error indicator and 2nd derivative (curvature) based error indicator are introduced and used for the solution of the Navier-Stokes equations.

NAVIER-STOKES EQUATIONS

The Navier-Stokes equations in conservation form may be written as [15]:

1. Mass Conservation Equation (the Navier-Stokes equations are presented in indicial notation):

$$\frac{\partial \rho}{\partial t} = \frac{1}{c^2}\frac{\partial p}{\partial t} = -\frac{\partial (U_i)}{\partial x_i}, \tag{1}$$

where c is the speed of sound, $U_i = \rho u_i$ in which ρ is density and u_i is velocity components. Obviously, for an incompressible flow the speed of sound approaches infinity and the left hand term approaches zero.

2. Momentum Conservation Equation:

$$\frac{\partial (U_i)}{\partial t} = -\frac{\partial (u_j U_i)}{\partial x_j} + \frac{\partial (\tau_{ij})}{\partial x_j} - \frac{\partial p}{\partial x_i} - \rho g_i, \tag{2}$$

where τ_{ij} is the deviatoric stress components obtained by:

$$\tau_{ij} = \mu \left(\frac{\partial u_i}{\partial x_j} + \frac{\partial u_j}{\partial x_i} - \frac{2}{3}\delta_{ij}\frac{\partial u_k}{\partial x_k} \right), \tag{3}$$

where μ is the dynamic viscosity and δ_{ij} is the kronecker delta:

$$\delta_{ij} = \begin{cases} 1 & i = j \\ 0 & i \neq j. \end{cases} \tag{4}$$

CHARACTERISTIC BASED SPLIT METHOD

The CBS (Characteristic Based Split) scheme is very similar to the original Chorin split or projection method, which is widely employed in incompressible flow calculations. Furthermore, it can be used for the solution of the compressible and incompressible flows. The temporal discretization scheme essentially contains three steps. In the first step, the intermediate velocity field is established, in the second step, the pressure is obtained from the continuity equation and, finally, the intermediate velocities are used to find the final velocity values. All three obtained equations can be spatially discretized by a standard Galerkin procedure [17]. After temporal and spatial discretization, the CBS-FEM yields to [17]:

$$\Delta \mathbf{U}^* = -\mathbf{M}_\mathbf{u}^{-1}\Delta t \left[(\mathbf{C}_\mathbf{u}\bar{\mathbf{U}} + \mathbf{K}_\mathbf{r}\bar{\mathbf{u}} - \mathbf{f}) \right.$$
$$\left. -\Delta t(\mathbf{K}_\mathbf{u}\bar{\mathbf{U}} + \mathbf{f}_\mathbf{s}) \right]^n, \tag{5}$$

$$(\mathbf{M}_\mathbf{p} + \Delta t^2 \theta_1 \theta_2 \mathbf{H})\Delta \bar{p} = \Delta t[\mathbf{G}\bar{\mathbf{U}}^n$$
$$+ \theta_1 \mathbf{G}\Delta\bar{\mathbf{U}}^* - \Delta t \theta_1 \mathbf{H}\bar{\mathbf{p}}^n - \mathbf{f}_p], \tag{6}$$

$$\Delta \bar{\mathbf{U}} = \Delta \bar{\mathbf{U}}^* - \mathbf{M}_u^{-1}\Delta t[\mathbf{G}^T(\bar{\mathbf{p}}^n + \theta_2 \Delta \bar{\mathbf{p}})$$
$$+ \frac{\Delta t}{2}\mathbf{P}\bar{\mathbf{p}}^n], \tag{7}$$

where the unknown variables $\mathbf{U}$ and p are spatially approximated, using shape functions N_u and N_p as usual, in a finite element context and θ_1, θ_2 are parameters for temporal discretization.

$$\mathbf{U} = \mathbf{N}_\mathbf{u}\bar{\mathbf{U}}, \qquad \Delta\mathbf{U} = \mathbf{N}_\mathbf{u}\Delta\bar{\mathbf{U}}, \qquad \Delta\mathbf{U}^* = \mathbf{N}_\mathbf{u}\bar{\mathbf{U}}^*,$$
$$p = \mathbf{N}_\mathbf{p}\bar{\mathbf{p}}, \qquad \mathbf{u} = \mathbf{N}_\mathbf{u}\bar{\mathbf{u}}, \tag{8}$$

and:

$$\mathbf{M}_u = \int_\Omega \mathbf{N}_\mathbf{u}^T \mathbf{N}_\mathbf{u} d\Omega, \tag{9}$$

$$\mathbf{C}_\mathbf{u} = \int_\Omega \mathbf{N}_\mathbf{u}^T (\nabla(\mathbf{u}\mathbf{N}_\mathbf{u})) d\Omega, \tag{10}$$

$$\mathbf{f} = \int_\Omega \mathbf{N}_\mathbf{u}^T \rho \mathbf{g} d\Omega + \int_\Gamma \mathbf{N}_\mathbf{u}^T \mathbf{t}^\mathbf{d} d\Gamma, \tag{11}$$

$$\mathbf{K}_\mathbf{r} = \int_\Omega \mathbf{B}^T \mu (\mathbf{I}_0 - \frac{2}{3}\mathbf{m}\mathbf{m}^T) \mathbf{B} d\Omega, \tag{12}$$

$$\mathbf{m} = [1 \quad 1 \quad 1 \quad 0 \quad 0 \quad 0]^T, \tag{13}$$

$$\mathbf{g} = [g_1 \quad g_2 \quad g_3]^T, \tag{14}$$

$$\mathbf{I}_0 = \begin{bmatrix} 2 & 0 & 0 & 0 & 0 & 0 \\ 0 & 2 & 0 & 0 & 0 & 0 \\ 0 & 0 & 2 & 0 & 0 & 0 \\ 0 & 0 & 0 & 1 & 0 & 0 \\ 0 & 0 & 0 & 0 & 1 & 0 \\ 0 & 0 & 0 & 0 & 0 & 1 \end{bmatrix}, \tag{15}$$

$$\mathbf{H} = \int_\Omega (\nabla \mathbf{N}_p)^T \nabla \mathbf{N}_p d\Omega, \tag{16}$$

$$\mathbf{M}_{\boldsymbol{\rho}} = \int_\Omega \mathbf{N}_p^T \left(\frac{1}{c^2}\right)^n \mathbf{N}_p d\Omega, \tag{17}$$

$$\mathbf{G} = \int_\Omega (\nabla \mathbf{N}_p)^T \mathbf{N}_u d\Omega, \tag{18}$$

$$\mathbf{f}_p = \Delta t \int_\Gamma \mathbf{N}_p^T \mathbf{n}^T [\bar{\mathbf{U}}^n + \theta_1(\Delta\bar{U}^* - \Delta t \nabla p^{n+\theta_2})] d\Gamma, \tag{19}$$

$$\mathbf{n} = [n_1 \quad n_2 \quad n_3]^T, \tag{20}$$

$$\mathbf{P} = \int_\Omega (\nabla(\mathbf{u}\mathbf{U}_u))^T \nabla \mathbf{N}_p d\Omega. \tag{21}$$

Each time step includes the following steps:

1. Obtaining $\Delta\bar{\mathbf{U}}^*$ from Equation 5;
2. Calculating $\Delta\bar{\mathbf{p}}$ from Equation 6;
3. Computing $\Delta\bar{\mathbf{U}}$ using Equation 7.

ADAPTIVE REFINEMENT

Adaptive refinement refers to the procedures that can be used to improve the efficiency and effectiveness of the FE computations by adaptively refining the FE mesh using error distribution obtained via the error estimation of an already existing solution. Adaptive methods were first introduced to finite element calculations by Babuska and Rheinbolt in the late 1970's [18,19]. Different adaptive strategies are introduced and used by other researchers to solve various problems. In this paper, the focus is on the h-refinement method in which the order of the elements are fixed but their size is adaptively changed such that the solutions of required accuracy are obtained.

In all adaptive refinement methods, it is necessary to clarify the objectives of refinement and specify a permissible error magnitude. This magnitude is obtained by a user from his/her engineering judgment. Three adaptive refinement methods used in this study are as follows.

Patch Recovery Based Error Estimator and Adaptive Refinement

The following L_2 norm is defined as the error estimator norm:

$$\|e\|_{L_2} = \int_\Omega (\mathbf{U} - \tilde{\mathbf{U}})^T (\mathbf{U} - \tilde{\mathbf{U}}) d\Omega, \tag{22}$$

in which $\mathbf{U}$ is the velocity vector approximated by the finite element solution and $\tilde{\mathbf{U}}$ is the velocity vector calculated by a Superconvergent Patch Recovery (SPR) algorithm [17]. In fluid dynamics problems, nodal values of velocities and pressure are the primary goal of computations. Therefore, nodal values are considered as superconvergent. As an error identifier, the relative L_2 error norm percentage is defined as:

$$\eta = \frac{\sqrt{\|\mathbf{e}\|_{L_2}}}{\sqrt{\|\mathbf{U}\|_{L_2}}} \times 100\%, \tag{23}$$

where:

$$\|\mathbf{U}\|_{L_2} = \int_\Omega \mathbf{U}^T \mathbf{U} d\Omega. \tag{24}$$

The error estimator presented in Equations 22 to 24 allows the global norm of the error to be determined and the errors occurring locally (at the element level) are also well represented. If these errors are within the limits prescribed by the analyst, then clearly the work is completed. More frequently, these limits are exceeded and refinement is necessary. In the optimal case, it is desirable that each element has the same error as:

$$\|\mathbf{e}\|_k < \bar{\eta}\left(\frac{\|\hat{\mathbf{u}}\|^2 + \|\mathbf{e}\|^2}{m}\right)^{1/2} = \bar{e}_m, \tag{25}$$

in which m is the number of elements and $\bar{\eta}$ is a user defined value (desired relative error). It is obvious that the elements in which the error norm is more than $\bar{e}_m$ need refinement. Therefore, the ratio ξ_k is defined as:

$$\frac{\|\mathbf{e}\|_k}{\bar{e}_m} = \xi_k. \tag{26}$$

Considering the polynomial order of approximation, one can estimate that:

$$\|\mathbf{e}\|_k = h_k^p, \tag{27}$$

where h_k is the current element size and p is the polynomial order of approximation. Equations 26 and 27 can be used to define the adapted element size as:

$$h_{\text{new}} = \xi_k^{-1/p} h_k, \tag{28}$$

in which h_{new} is the new element size.

First Derivative (Gradient) Based Error Indicator and Adaptive Refinement

The nature of fluid flow problems away from boundaries is almost hyperbolic. For hyperbolic problems, the error can be estimated in terms of the gradient of the solution in the computational domain. In such cases the error can be considered as [17]:

$$h\frac{\partial \phi}{\partial n} = \beta, \tag{29}$$

where n is the direction of maximum gradient, h is the element size (minimum size) in the same direction and β is a user defined constant. The above expression can be used to determine the minimum element size at all nodes or other points of consideration. At every point, a maximum element size should be determined.

Second Derivative Based Error Indicator and Adaptive Refinement

A second derivative based error indicator is introduced using a different point of view from that of the gradient based error indicator described before and an approach is used in which the error value is constant in each element.

Determination of error indicators in linear elements is achieved by considering the so-called interpolation error. Consider a one-dimensional element of length h over which a scalar function ϕ is approximated. It is clear that the error in ϕ using linear elements is of the order $O(h^2)$ and can be written as [17]:

$$e = \phi - \phi^h = ch^2\frac{d^2\phi}{dx^2} \approx ch^2\frac{d^2\phi^h}{dx^2}, \tag{30}$$

where ϕ^h is the finite element solution and c is a constant.

As the nodal values are always more accurate than those elsewhere, it can be tried to find an element subdivision of how to maintain an equal distribution of errors using the following equation:

$$h^2\frac{d^2\phi^h}{dx^2} = \gamma, \tag{31}$$

in which the arbitrary constant γ in Equation 31 can be interpreted as limiting interpolation error. The element subdivision can, therefore, be sought such that:

$$h^2\frac{d^2\phi^h}{dx^2} \le e_p, \tag{32}$$

where e_p is the user-specified error limit. In two and three dimensions, the second derivatives (or curvatures) are tensor valued quantities and given as $\partial^2\phi/\partial x_i \partial x_j$. Such definitions require the determination of the principal values and directions. These principal directions are necessary for element elongation, which is an essential property of this method. If X_I and X_2 are the directions of the minimum and maximum principal values of the curvatures, then for an equal distribution of interpolation error we can write for each node:

$$h_{\min}^2\left|\frac{\partial^2\phi}{\partial X_2^2}\right| = h_{\max}^2\left|\frac{\partial^2\phi}{\partial X_1^2}\right| = \gamma, \tag{33}$$

which gives the stretching ratio s as:

$$s = \frac{h_{\max}}{h_{\min}} = \sqrt{\frac{\left|\frac{\partial^2\phi}{\partial X_2^2}\right|}{\left|\frac{\partial^2\phi}{\partial X_1^2}\right|}}. \tag{34}$$

NUMERICAL EXAMPLES

A lid-driven cavity flow problem is considered here as shown in Figure 1. The top lid of a square and closed cavity (1.0 m × 1.0 m) is assumed to move in its plane with certain uniform prescribed velocity (1.0 m/s). All other walls are assumed to be stationary with zero velocity components imposed on them (no slip walls). The flow is considered laminar and incompressible. The boundary conditions for the velocities are $u_x = 0.0$, $u_y = 0.0$ on the boundaries AB, BC, CD and $u_x = 1.0$ m/s and $u_y = 0.0$ on the boundary AD. The pressure boundary condition is $p = 0$ at point E.

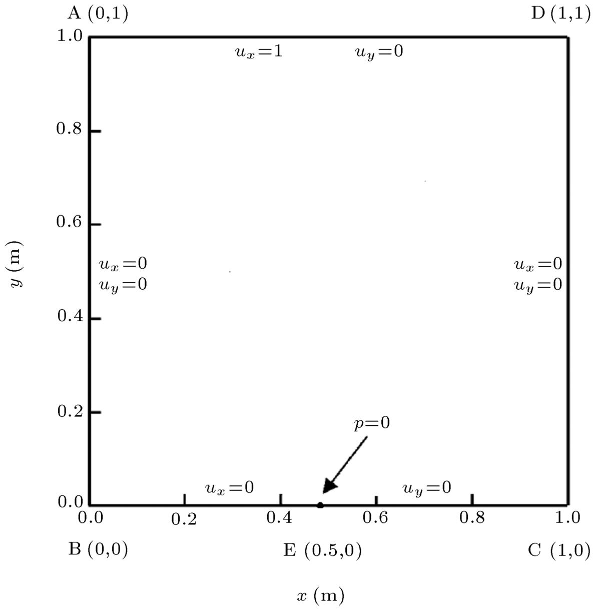

Figure 1. Lid-driven cavity and its boundary conditions.

The problem is solved for a Reynolds number with the definition of Reynolds number as:

$$\mathrm{Re} = \frac{\rho u l}{\mu}, \tag{35}$$

where characteristic velocity u and characteristic length l are chosen 1.0 m/s and 1.0 m for this example, respectively and ρ and μ denote the density and dynamic viscosity of the fluid. A semi implicit scheme with $\theta_1 = \theta_2 = 0.5$ is considered.

Solution of Lid Driven Cavity Problem with Patch Recovery Based Refinement

Three different triangular meshes are considered as illustrated in Figure 2. A driven cavity problem with Re = 5000 is solved. For comparison, the element size in each mesh is almost equal and the sizes of the elements in these meshes are 0.1 m, 0.05 m and 0.03 m, respectively. The relative error percentage, presented by Equation 23, in these meshes is 14.6, 10.65 and 7.76, respectively.

The convergence rate is illustrated in Figure 3 and, as desired, the convergence rate is lower than 1. The reason is the presence of singularities in the cavity [17].

Here, a modified form of the original superconvergent patch recovery is used to produce superconvergent velocities, which are subsequently used for error estimate and adaptive refinement strategy. The original superconvergent patch recovery uses polynomials of the same order as those of the shape function. Here, the polynomial basis of one order higher than the shape functions are used to improve the effectiveness

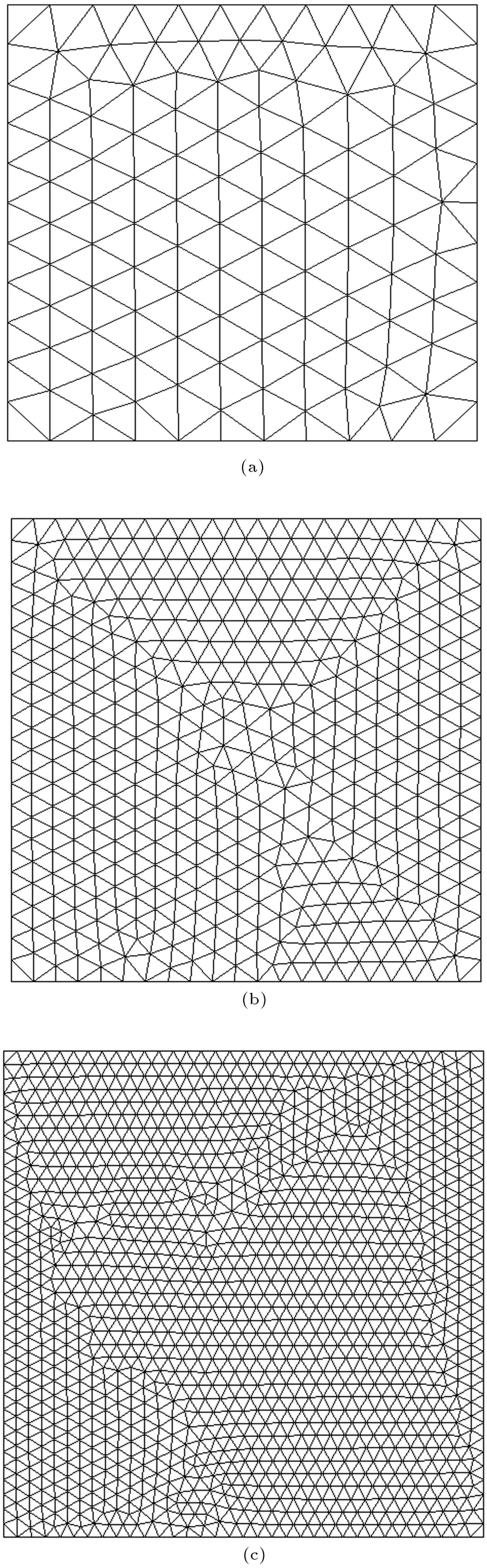
(a)

(b)

(c)

Figure 2. Three kinds of mesh.

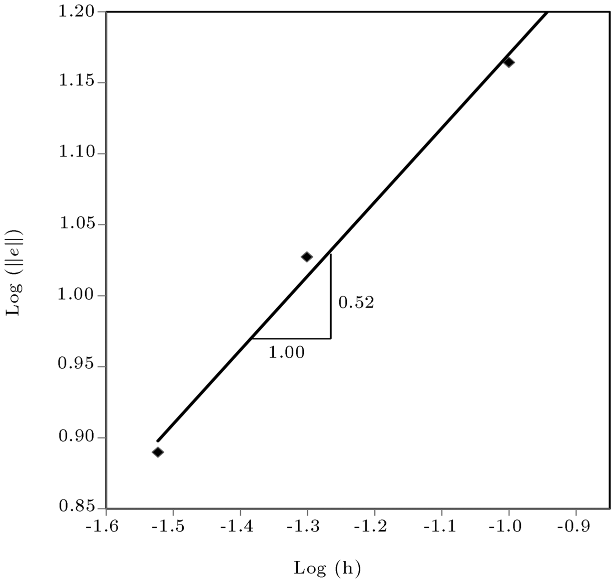

Figure 3. Error norm-mesh size relation in cavity problem.

of the procedure, leading to a polynomial basis of second order. This, however, meant that the patch of elements should be extended beyond the neighboring elements if the number of neighboring elements was less than the number of terms in the second order polynomial basis. The mesh generation program in which the local element size can be specified, is utilized to design a new mesh for which the re-analysis is carried out.

The lid-driven cavity problem is solved using Mesh 2, illustrated in Figure 2, and the error norm of each element is obtained. Figure 4 illustrates the distribution of ξ_k with a $\bar{\eta} = 0.2$ in a line representation. Pressure contours and streamlines obtained by this mesh, using CBS-FEM, are presented in Figures 5 and 6, respectively.

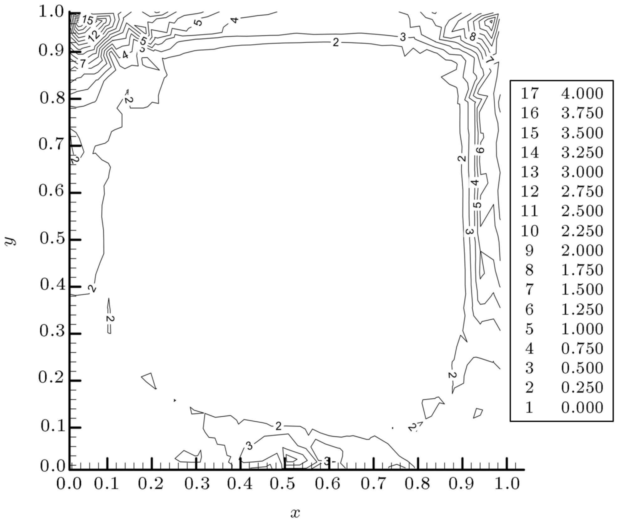

Figure 4. Distribution of ξ_k with a $\bar{\eta} = 0.2$.

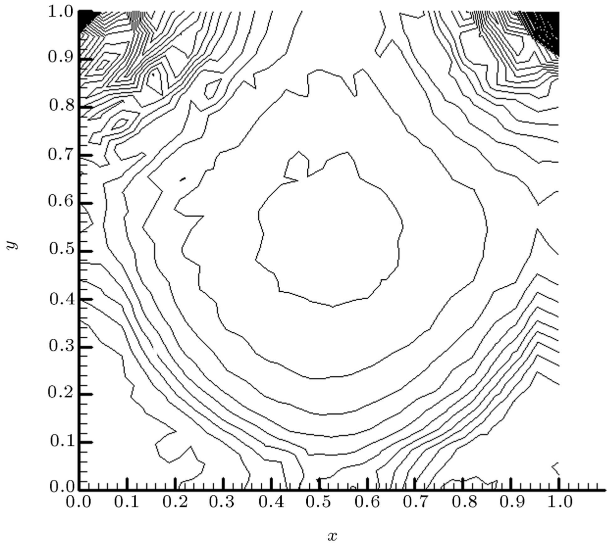

Figure 5. Pressure contours for Mesh 2.

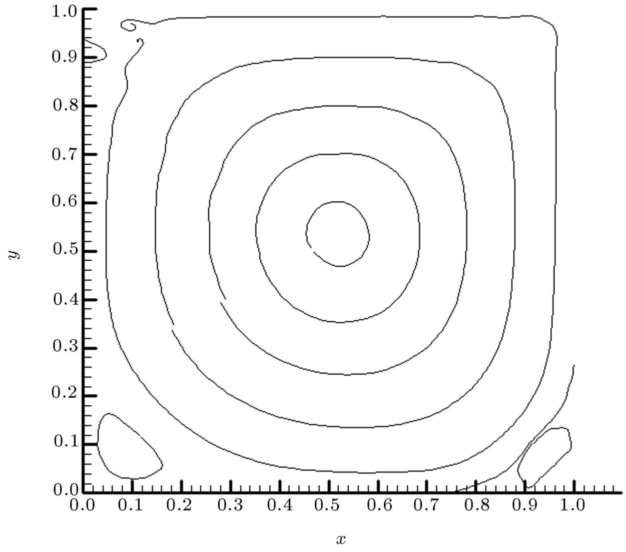

Figure 6. Stream line for Mesh 2.

Using adaptive refinement, two new meshes are generated. Mesh 4 is constructed considering the minimum element length equal to 0.01 m and the maximum element length equal to 0.05 m with $\bar{\eta} = 0.2$ and Mesh 5 is treated considering these limits with $\bar{\eta} = 0.1$. Mesh 4 and Mesh 5 are illustrated in Figures 7 and 8, respectively.

Mesh 5 with 2376 nodes and 4508 elements is applied for the Lid-driven cavity flow problem with Re = 5000 pressure contours. Streamlines are presented in Figures 9 and 10.

Lid Driven Cavity with Gradient Based Refinement

Gradient based refinement adaptive refinement is used to generate new mesh for a lid-driven cavity problem

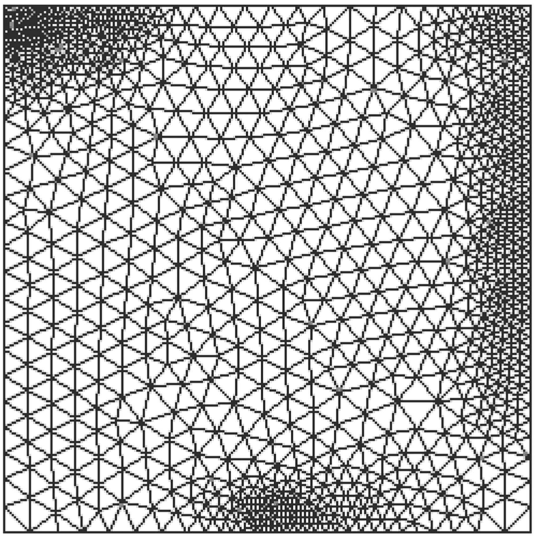

Figure 7. Mesh 4 with $\bar{\eta} = 0.2$.

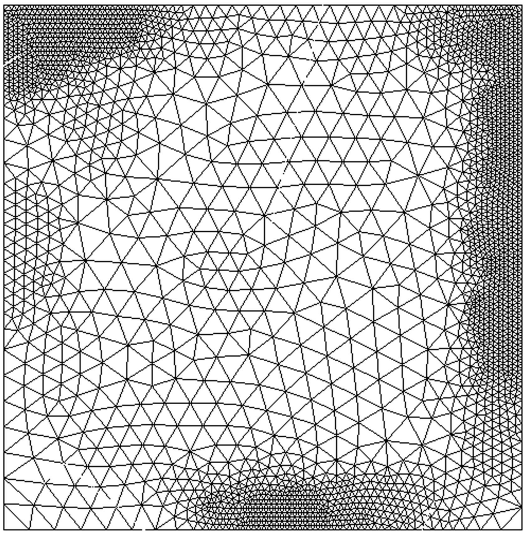

Figure 8. Mesh 5 with $\bar{\eta} = 0.1$.

with Re = 5000. Using this method, the refined meshes are obtained with different error criteria.

Figures 11 and 12 are obtained with two different $\beta = 5$ and $\beta = 2$ respectively. The maximum and minimum values of element lengths are considered 0.05 m and 0.01 m, respectively.

The lid-driven cavity problem is solved using Mesh 7, illustrated in Figure 12. Pressure contours and streamlines are presented in Figures 13 and 14, respectively.

Lid Driven Cavity with Second Derivative (Curvature) Based Method

A refined mesh, using a second derivative based method, is generated, while the initial mesh is Mesh 2 and the error criteria is considered $\gamma = 0.913$. The

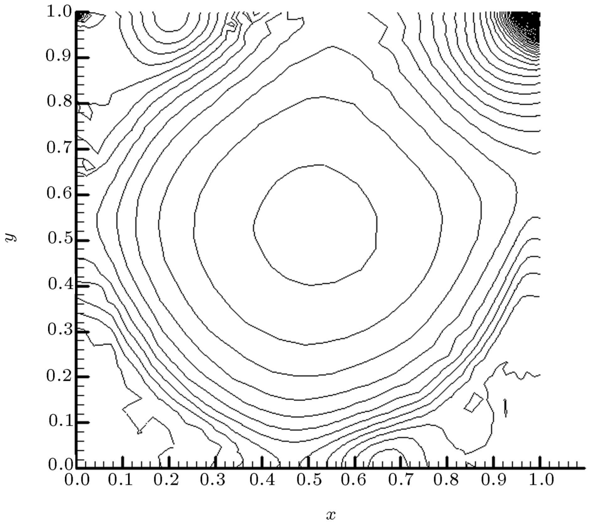

Figure 9. Pressure contours for Mesh 5.

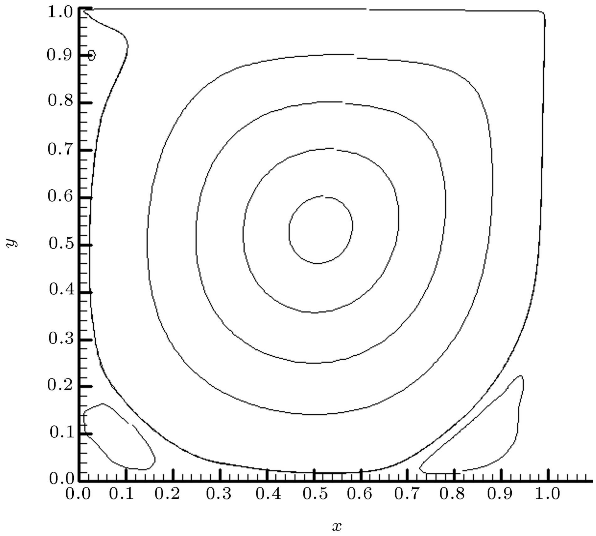

Figure 10. Streamlines for Mesh 5.

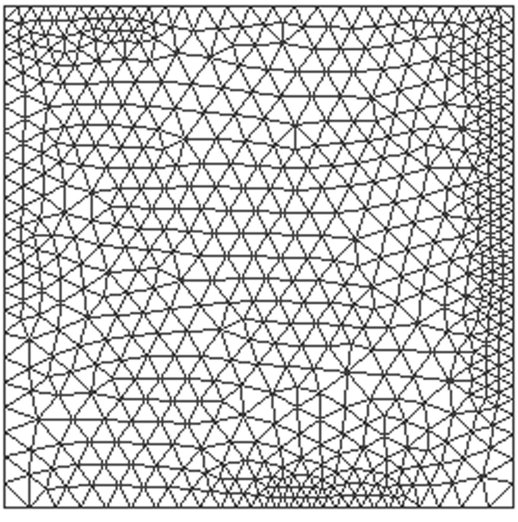

Figure 11. Mesh 6 with $\beta = 5$.

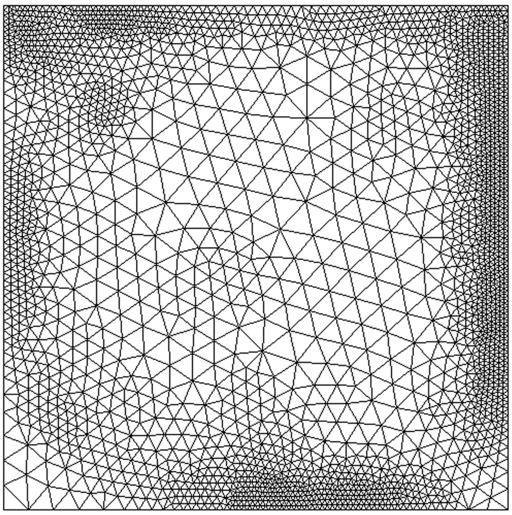

Figure 12. Mesh 7 with $\beta = 2$.

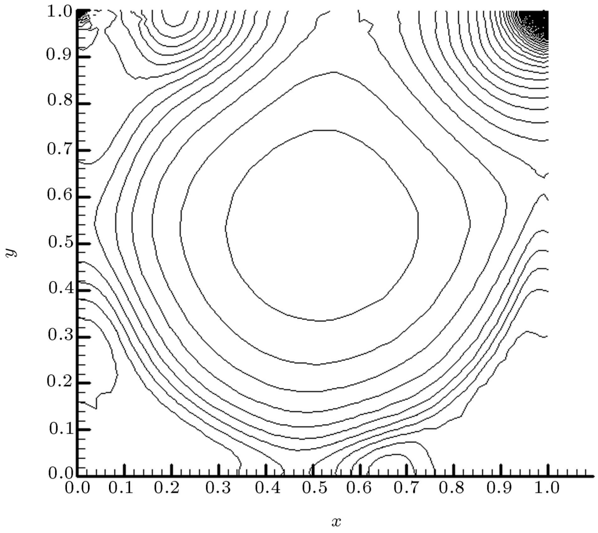

Figure 13. Pressure contours for Mesh 7.

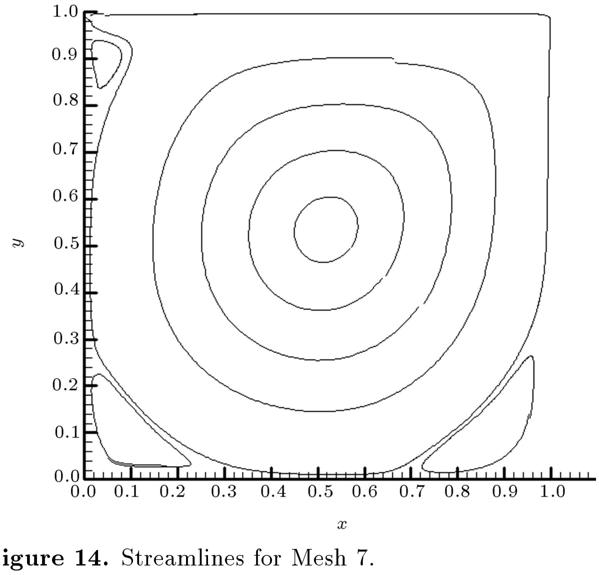

Figure 14. Streamlines for Mesh 7.

generated mesh with 2372 nodes and 4483 elements is presented in Figure 15.

The maximum and minimum element characteristic lengths are considered to be 0.05 m and 0.01 m, respectively, and the elongation ratio is set to 1. The pressure contours and streamlines obtained by the solution of the lid-driven cavity flow problem with Re = 5000 are illustrated in Figures 16 and 17, respectively.

To emphasize the ability of this method to generate elongated elements, the elongation ratio for the problem is considered as 3.0 and error criteria $\gamma = 0.77$. The generated mesh with 2378 nodes and 4571 elements is illustrated in Figure 18.

The Lid-driven cavity problem is solved with Mesh 9 and the obtained results are illustrated in Figures 19 and 20.

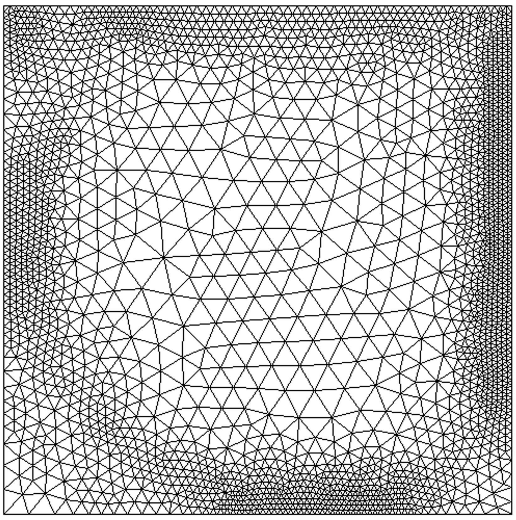

Figure 15. Mesh 8 generated by second derivative based method.

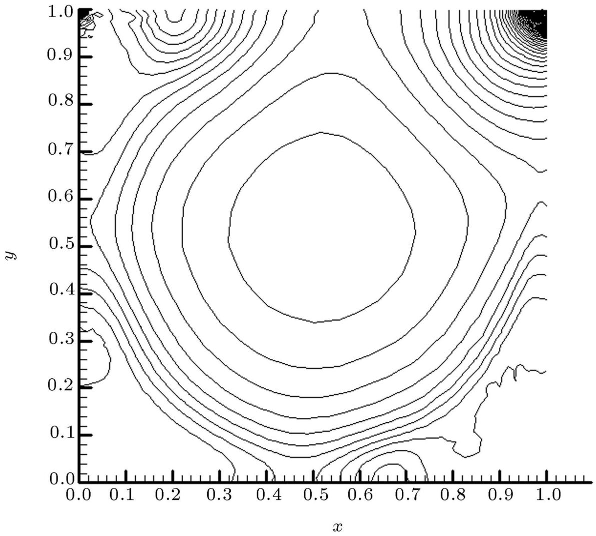

Figure 16. Pressure contours for Mesh 8.

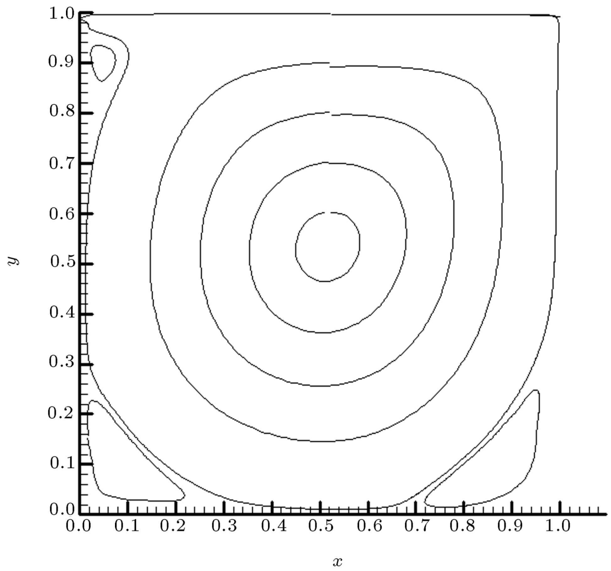

Figure 17. Streamlines for Mesh 8.

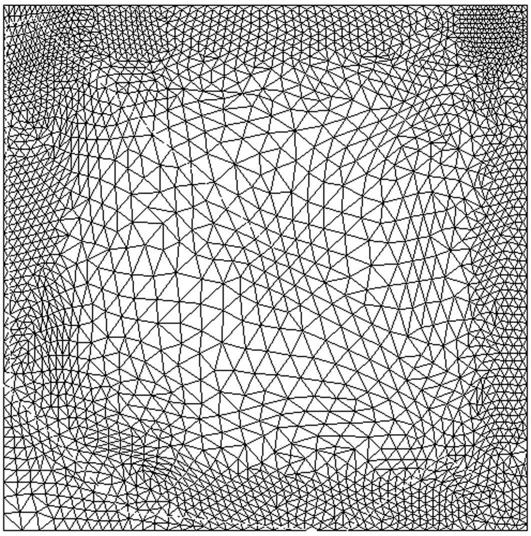

Figure 18. Mesh 9; adapted mesh with elongated elements.

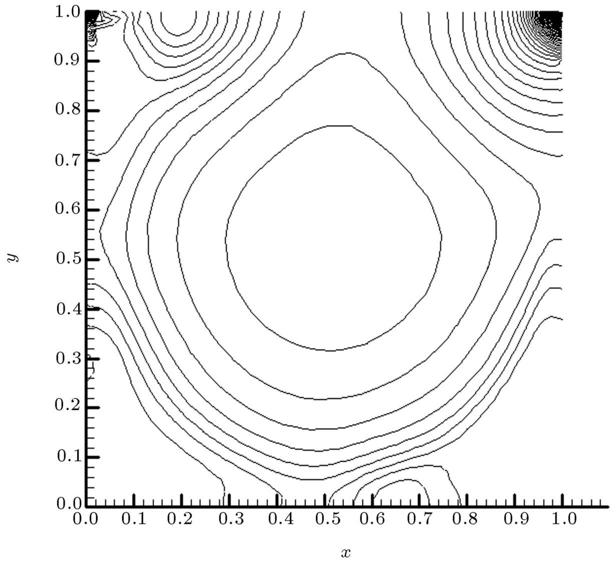

Figure 19. Pressure contours for Mesh 9.

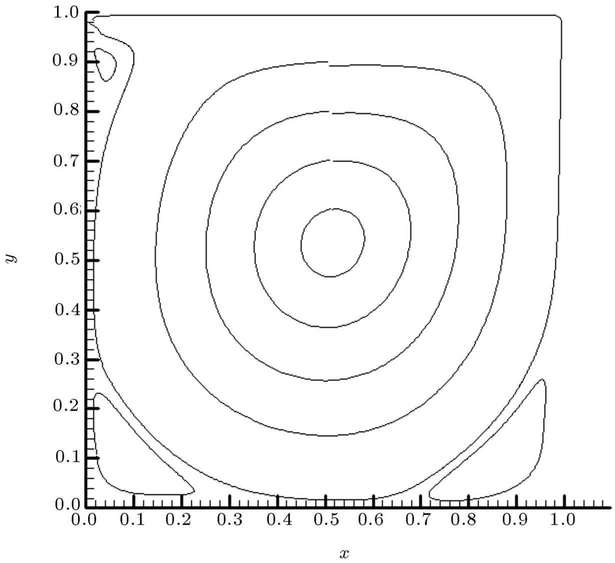

Figure 20. Streamlines for Mesh 9.

Horizontal velocity profiles at $x = 0.5$ m obtained by the CBS method are presented for Mesh 2, Mesh 5, Mesh 7, Mesh 8 and Mesh 9 in Figure 21. It is seen that the results of the adapted and non-adapted meshes are considerably different, especially in the vicinity of the walls. It is further noted that the results obtained using different adaptive techniques are almost similar.

The results obtained using these adaptive refinement techniques compare well with those of the previous published reports. Ghia et al. [20] carried out a detailed investigation for the lid-driven cavity problem. The horizontal velocity profile for Re = 5000 obtained by them is illustrated in Figure 22 for comparison purposes.

The Super-convergent Patch Recovery (SPR) based technique needs more computational effort than others, whereas the gradient based algorithm needs the least computational effort. Unlike these two techniques, the curvature based adaptive refinement is capable of generating elongated elements.

CONCLUSIONS

Three adaptive refinement methods based on different concepts, namely, Superconvergent Patch Recovery (SPR) based refinement, gradient based refinement and curvature (2nd derivative) based refinement, have been revisited, tested and compared. A Characteristic Based

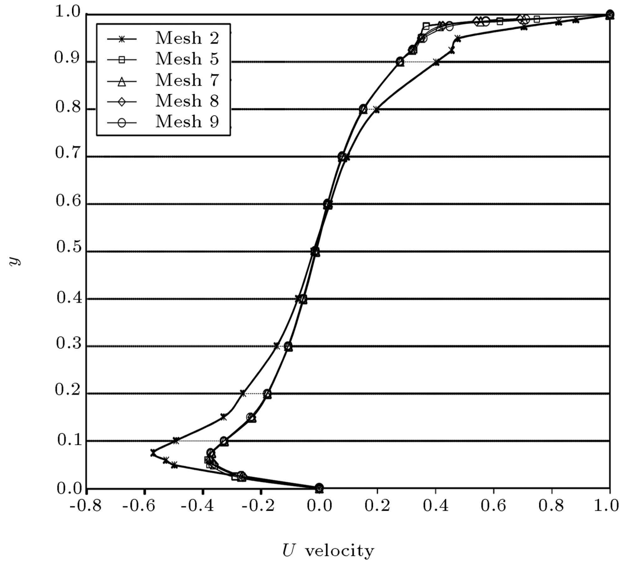

Figure 21. Comparison of horizontal velocity along mid-vertical line profiles.

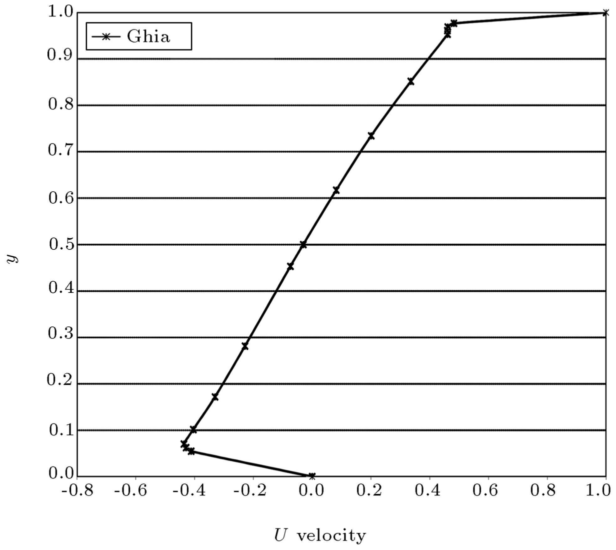

Figure 22. Reference horizontal velocity along mid-vertical line profiles by Ghia [20].

Split (CBS) method is carried out to solve Navier-Stokes equations. The results obtained by these three methods are almost similar. It can be mentioned that the superconvergent patch recovery based technique has more computational effort than others, whereas the gradient based algorithm has the least computational effort and curvature based adaptive refinement enjoys the property of being able to generate elongated elements.

REFERENCES

1. Zienkiewicz, O.C. and Zhu, J.Z. "The superconvergent patch recovery and a posteriori error estimation. Part I: The recovery technique", *Int. J. Numer. Methods Eng.*, **33**, pp. 1331-1364 (1992).
2. Zienkiewicz, O.C. and Zhu, J.Z. "The superconvergent patch recovery and a posteriori error estimation. Part II: Error estimates and adaptivity", *Int. J. Numer. Methods Eng.*, **33**, pp. 1365-1382 (1992).
3. Zienkiewicz, O.C. et al. "Superconvergent recovery technique, some further tests", *Comm. Appl. Sci. Eng.*, **9**, pp. 251-258 (1993).
4. Zienkiewicz, O.C. and Zhu, J.Z. "Superconvergence and the superconvergent patch recovery", *Journal of Finite Element in Analysis and Design*, **19**, pp. 11-23 (1995).
5. Lee, T. et al. "Super convergent stress recovery technique with equilibrium constraints", *Int. J. Numer. Methods Eng.*, **40**, pp. 1139-1160 (1997).
6. Tenchev, R.T. "A study of the accuracy of some FEM stress recovery schemes for 2D stress concentration problems", *Finite Elem. Anal. Des.*, **29**, pp. 105-119 (1998).
7. Perala, M.R. "A patch recovery method based on velocity-pressure formulation for 2D stokes and Navier-Stokes problems", *5th Congress on Computational Mechanics*, Vienna, Austria (2002).
8. Almeida, R.C. et al. "Adaptive finite element computational fluid dynamics using an anisotropic error estimator", *Comput. Methods Appl. Mech. Engrg.*, **182**, pp. 379-400 (2000).
9. Cao, J. "Application of a posteriori error estimation to finite element simulation of compressible Navier-Stokes flow", *Computers & Fluids*, **34**, pp. 991-1024 (2005).
10. Zienkiewicz, O.C. et al. "An 'upwind' finite element scheme for two-dimensional convective transport equations", *Int. J. Numer. Methods Engrg.*, **11**, pp. 131-143 (1977).
11. Brooks, A.N. and Hughes, T.J.R. "Streamlines upwind/Petrov-Galerkin formulations for convection dominated flows with particular emphasis on the incompressible Navier-Stokes equations", *Comput. Methods Appl. Mech. Engrg.*, **32**, pp. 199-259 (1982).
12. Donea, J. "A Taylor-Galerkin method for convective transport problems", *Int. J. Numer. Methods Engrg.*, **20**, pp. 101-119 (1984).
13. Donea, J. et al. "A generalized Galerkin method for steady state convection-diffusion problems with application to quadratic shape function", *Comp. Meth. Appl. Mech. Eng.*, **48**, pp. 25-43 (1985).
14. Onate, E. "Derivation of stabilized equation for numerical solution of advective-diffusive transport and fluid flow problems", *Comp. Meth. Appl. Mech. Eng.*, **151**, pp. 233-265 (1998).
15. Chorin, A.J. "Numerical solution of Navier-Stokes equations", *Math. Comp.*, **22**, pp. 745-62 (1968).
16. Chorin, A.J. "On the convergence of discrete approximation to the Navier-Stokes equations", *Math. Comp.*, **23**, pp. 341-53 (1969).

17. Zienkiewicz, O.C. and Taylor, R.L. "The Finite element methods, Vol. 3: Fluid Dynamics", *Butterworth-Heinemann*, 5th Ed., Oxford, UK (2000).

18. Babuska, I. and Rheinboldt, C. "A-posteriori error estimates for the finite element method", *Int. J. Numer. Methods Eng.*, **12**, pp. 1597-615 (1978).

19. Babuska, I. and Rheinboldt, C. "Adaptive approaches and reliability estimates in finite element analysis", *Comput. Methods Appl. Mech. Eng.*, **17-18**, pp. 519-540 (1979).

20. Ghia, U. et al. "High resolutions for incompressible flow using the Navier-Stokes equation and multigrid methods", *J. Comput. Phys.*, **48**, pp. 387-411 (1982).